Proceedings of the 3rd World Congress on Mechanical, Chemical, and Material Engineering (MCM'17)
Rome, Italy – June 8 – 10, 2017
Paper No. HTFF 126
ISSN: 2369-8136
DOI: 10.11159/htff17.126

Numerical Simulation of Metal Hydride Hydrogen Storage Device with Pin Fin Tube Heat Exchanger

Vikas Keshari, M. P. Maiya
Refrigeration and Air Conditioning Laboratory
Department of Mechanical Engineering
Indian Institute of Technology Madras
Chennai-600036, India
me15s026@smail.iitm.ac.in; mpmaiya@iitm.ac.in

Abstract **-** Absorption of hydrogen gas into a metal hydride is an exothermic process. Heat released during the reaction must be extracted from the metal hydride hydrogen storage device to enhance the absorption rate of hydrogen. Previous studies suggest that insertion of an effective heat exchanger inside the storage device improves the absorption rate of hydrogen. In our present study, six different pin fin tube heat exchanger designs are proposed. Individual charging time of designed heat exchangers is found out numerically and a comparative study is carried out among all of them. COMSOL Multiphysics 4.3b is used for designing and simulating the models. Among the proposed designs, a final design is selected based on the least charging time and detailed 3-D mathematical model is developed for further study of absorption process inside the storage device. Influence of the hydrogen supply pressure on the charging time of the storage device has been examined. It is found that higher supply pressure of hydrogen gas reduces the charging time of the storage device. Variation of bed temperature and concentration along the axial distance of the storage device has also been investigated. It is found that mid part of the device is having constant temperature as well as concentration profile at any time interval while parts near the flange portions saturate earlier than middle region. The absorption process takes 727 s to absorb 1.4 wt% of hydrogen at the operating conditions of 15 bar, 298 K and 0.113 Kg/s. This numerical study suggests that the good selection of heat exchanger geometry is important for rapid absorption process inside the storage device.

Keywords**:** $LaNi_5$, Heat and mass transfer, Heat exchanger, Copper pin fin, Charging time, COMSOL Multiphysics

1. Introduction

World-wide demand for energy is rapidly increasing due to growing population and living standards. At present, our energy needs are fulfilled by fossil fuels such as crude oil, coal and natural gas. However, continuous depletion of these fuels and increasing level of global warming gases as well as air pollutants have accelerated the demand for the development of clean and sustainable energy technology. Renewable energy sources such as solar, wind, geothermal and biomass can not be used for wide spread applications due to their intermittent nature and high initial investments. With this background hydrogen can be considered as a promising and clean energy carrier for future. Hydrogen fuel offers many benefits such as abundant availability and burning without any harmless production. The major obstruction to bring hydrogen economy into reality is its safe and cost effective storage. Conventionally, high pressure gas compression and liquefaction (cryogenic storage) methods are used to store the hydrogen. Gas compression method has some drawbacks such as cost of compression, low storage density and explosion risk. Liquefaction method has also some disadvantages such as cost of storage and bulky insulation to prevent boil-off the liquid hydrogen. An alternative solution seems to be hydrogen storage in hydride form which has several advantages such as volumetric storage density, better safety and cost effectiveness. Hydride form of storage method requires a metal alloy to absorb and hold large amounts of hydrogen by chemical bonding. During chemical reaction between hydrogen and metal alloy significant amount of heat is generated. Due to the low thermal conductivity of metal hydride powder, heat removal rate retards and increases the charging time of the storage device. Hence, internal heat transfer enhancement is important which can be achieved by integrating a heat exchanger inside the storage device.

Numerical modelling of metal hydride hydrogen storage system has received considerable attention over last few decades to improve the heat and mass transfer characteristics of the storage device. Singh et al. [1] presented the numerical model of hydrogen storage device incorporating a heat exchanger tube brazed with radial circular copper fins on its periphery. The model was validated with experimental work. Garrison et al. [2] performed simulation for the optimization of heat exchanger design by varying the fin and tube parameters. Transverse and longitudinal fin designs are considered for the numerical model. Ma et al. [3] studied the transient reaction process in a finned multi-tubular metal hydride tank by different fin configurations and operating conditions. Wang et al. [4] simulated a 3-D mathematical model to study the transient heat and mass transfer in a cylindrical metal hydride tank integrated with a helical coil heat exchanger. Mellouli et al. [5] numerically investigated a 2-D mathematical model of metal hydride tank incorporating a finned spiral tube heat exchanger.

As we can see that all the above published numerical and experimental works indicate that heat transfer rate is the key factor for the absorption rate of hydrogen inside the metal hydride system. A number of methods are developed to increase the heat transfer rate such as embedding a copper wire net structure, mixing of hydride alloy with expanded graphite and placing a heat exchanger inside the hydride system. Among all these methods, predominant method is the use of heat exchanger. Different type of heat exchangers such as spiral-tube heat exchanger, shell and tube heat exchanger, plate fin tube heat exchanger and helical coil heat exchanger are used by researchers. However, a numerical study of coupled heat and mass transfer process in hydride system incorporating a pin fin tube heat exchanger has not been explored. The aim of the study is the investigation of hydrogen absorption process in the storage device.

2. Heat exchanger Designs

Six different 3-D designs of heat exchangers and their sectional views are given in figure 1. Designs are built using COMSOL Multiphysics 4.3b. Storage device comprises HX design inside the cylindrical vessel. Device is designed for 1 kg of LaNi5 hydriding alloy. Required total volume of the vessel is the combination of HX volume, 1 kg of LaNi5 alloy and its expansion volume (22.4% for LaNi5). Tubes and cylindrical pin fins made of copper are used to make heat exchanger assemblies. Pin fins are generally used in refrigeration industry. Pin fin diameter and tube thickness are selected according

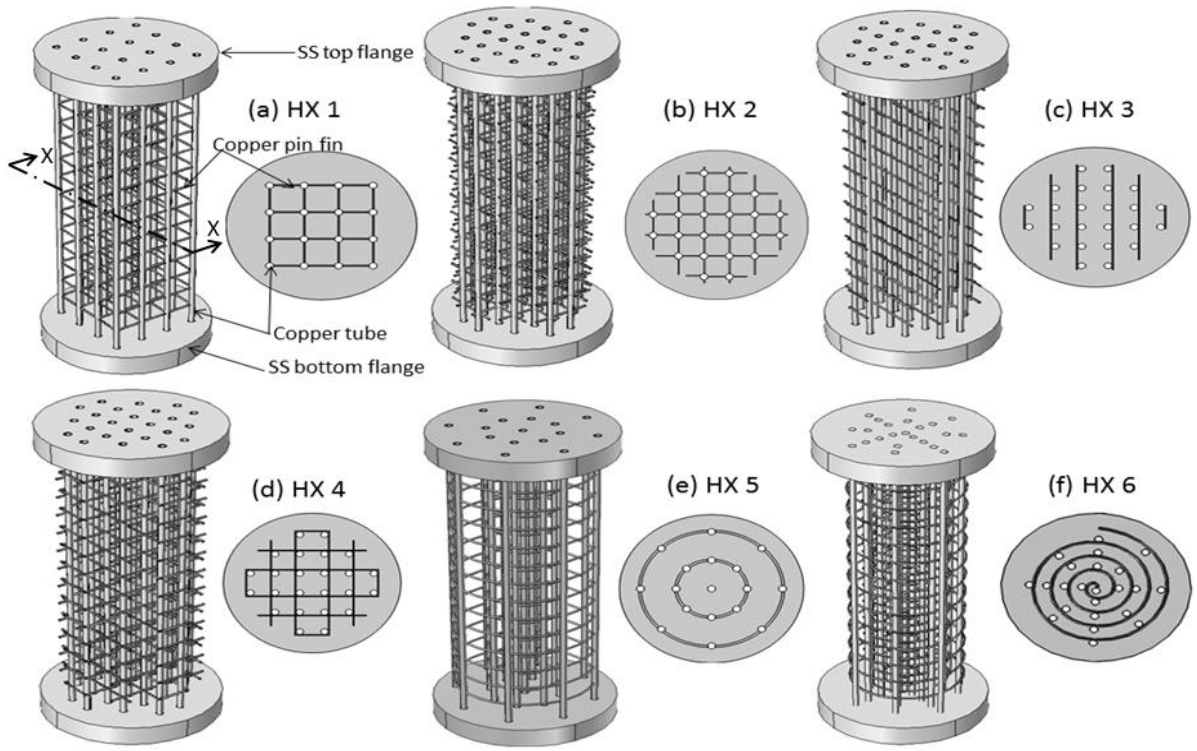

Fig. 1: Schematic of various HX designs and their top views at mid-plane.

to weight as well as volume of the heat exchanger, ease of availability in the market and heat transfer capability. There are two ways to attach pin fin on the copper tube (1) centre to centre and (2) side by side attachment. Both the attachments are used in our study. Centre to centre attached fins have slightly better efficiency in comparison to side by side attached fins but its manufacturability is difficult. Metal hydride (porous material) bed is packed uniformly between fins and tubes inside the storage device. SS headers are placed on the top of the flange portions for the distribution of water during cooling process. Water enters in the inlet header and distributed to the tubes for removal of the released heat during reaction and again collected in outer header for leaving the heat exchanger. Distributed mass flow rate of water depends upon the number of tubes used in a particular design. Inlet flow rate of water is kept constant as 0.113 Kg/s for each case. 13 pin fin arrays are used in every design of HX. One pin fin array for HX design 2 is shown in figure 2(b). All the HX designs are built with the same base dimensions. These dimensions are tube inner/outer diameter, tube length, Pin fin diameter, flange thickness, flange diameter, heat exchanger height and fin pitch.

2. Mathematical Model

Experimental work is considered to be costly, so all the HX designs are solved numerically for comparing their performance. For HX design 2, one pin fin array and model used for simulation is shown in figure 2(b) and (c). Following assumptions are made for the simplification of the numerical study.

1. Solid and gas phase of the bed are having the same instantaneous temperature everywhere inside the storage device.
2. Homogenous and isotropic bed is considered.
3. Convection and radiation heat transfers are neglected. Only conduction heat transfer is considered inside the bed.
4. Thermo-physical properties of the hydride bed are not changing with change in temperature, pressure and concentration.
5. Hydrogen is considered as perfect gas.
6. Expansion of bed is neglected during simulation.
7. Perfect thermal contact exists between bed and tube as well as bed and fin.

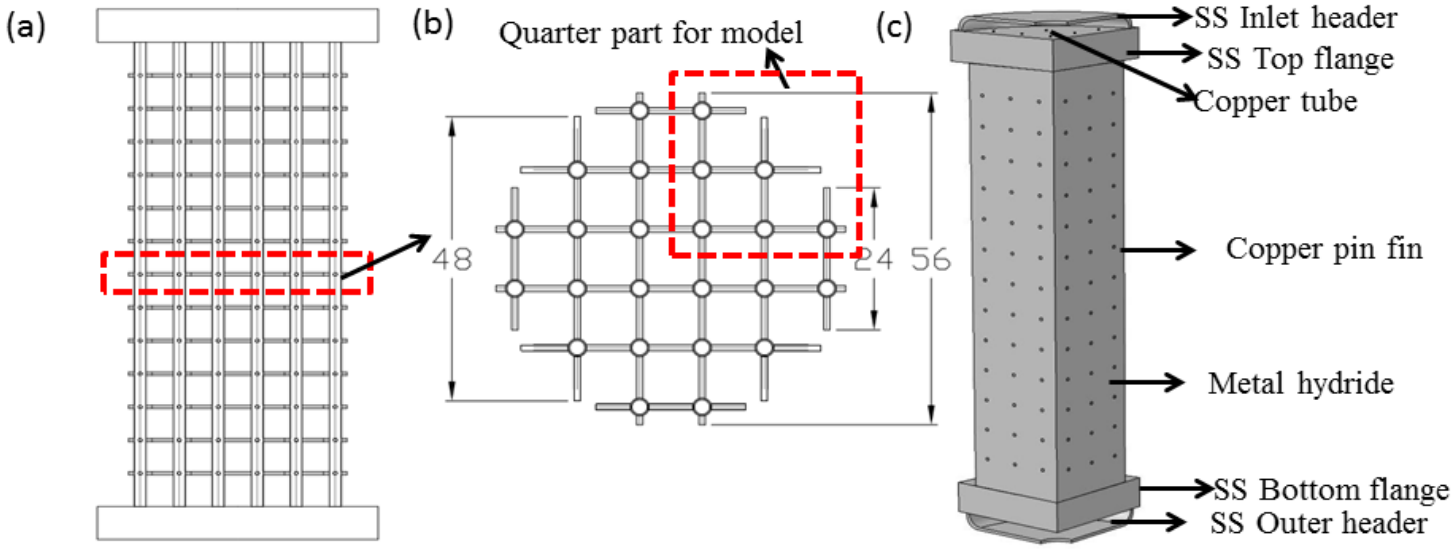

Fig. 2: Schematic of HX design 2 (a) front view (b) one pin fin array and (c) model used for simulation.

2.1. Volume Averaged Mass Balance Equation

Volume averaged mass balance equation for the MH in the 3-D Cartesian coordinates is given as [1]:

$$(1-\varepsilon)\frac{\partial \rho}{\partial t} = \dot{m} + (1-\varepsilon)\frac{\partial}{\partial x}\left(D\frac{\partial \rho}{\partial x}\right) + (1-\varepsilon)\frac{\partial}{\partial y}\left(D\frac{\partial \rho}{\partial y}\right) + (1-\varepsilon)\frac{\partial}{\partial z}\left(D\frac{\partial \rho}{\partial z}\right) \quad (1)$$

Where, ρ represents the density of MH, D signifies the mass diffusion coefficient, $\dot{m}$ denotes the mass of hydrogen that is absorbing in MH with time and ε denotes the porosity of metal alloy. The 2nd, 3rd, and 4th terms in RHS of the Eq. (1) are diffusive transport due to concentration variation within the bed. Diffusion coefficient (D) is expressed as follows:

$$D = 3.4 \times 10^{-07} \exp\left(\frac{-3365.485}{T}\right) \tag{2}$$

2.2. Volume Averaged Energy Balance Equation

Energy equation represents the temperature variation inside the hydrogen storage device. Energy equation for the MH bed system (porous material) in 3-D Cartesian coordinates is written as [1]:

$$(\rho c_p)_{eff} \frac{\partial T}{\partial t} = \frac{\partial}{\partial x}\left(k_{eff} \frac{\partial T}{\partial x}\right) + \frac{\partial}{\partial y}\left(k_{eff} \frac{\partial T}{\partial y}\right) + \frac{\partial}{\partial z}\left(k_{eff} \frac{\partial T}{\partial z}\right) - (1-\varepsilon)\dot{m}\,\Delta H \tag{3}$$

Effective volumetric heat capacity $(\rho c_p)_{eff}$ and effective thermal conductivity k_{eff} are given as follows:

$$\left(\rho c_p\right)_{eff} = \varepsilon(\rho c_p)_{gas} + (1-\varepsilon)(\rho c_p)_{mh} \tag{4}$$

$$k_{eff} = \varepsilon\, k_{gas} + (1-\varepsilon) k_{mh} \tag{5}$$

In Eq. (3), first term is transient variation in bed temperature and RHS last term is the heat generation due to the reaction. Left out terms denote the conduction heat transfer through bed. ΔH is known as heat of formation for MH.

2.3. Energy Balance Equation for the Pin Fins, Tubes and Headers Steel Portion

Energy balance equation for the pin fins, tubes, and headers steel portion is written as Eq. (3), by removing the heat generation term in RHS.

2.4. Governing Equation for Cooling Fluid of Heat Exchanger Tube

$$(\rho c_p)_f \frac{\partial T_f}{\partial t} + (\rho c_p)_f \vec{u}\, \mathrm{grad} T_f = \mathrm{div}(k_f\, \mathrm{grad} T_f) \tag{6}$$

$\vec{u}$ is the velocity of the fluid. Due to this velocity, energy is transferred physically from one place to another place.

2.5. Reaction Kinetics

The amount of hydrogen absorbed and desorbed by the MH per unit time and volume is written as $\dot{m}_a$ and $\dot{m}_d$ respectively and can be given as [3]:

$$\text{For hydriding:} \quad \dot{m}_a = C_a \exp\left(\frac{-E_a}{RT}\right) \ln\left(\frac{P}{P_{eq}}\right)(\rho_{sat} - \rho_{t,a}) \tag{7}$$

$$\text{For dehydring:} \quad \dot{m}_d = C_d \exp\left(\frac{-E_d}{RT}\right) \ln\left(\frac{P - P_{eq}}{P_{eq}}\right)\left(\rho_{t,d} - \rho_{alloy}\right) \tag{8}$$

Where, ρ_{sat} is the saturated density and ρ_{alloy} is the MH alloy density. $\rho_{t,a}$ and $\rho_{t,d}$ are the transient density for absorption and desorption processes. Equilibrium pressure P_{eq} inside the storage device can be given by vant's Hoff relationship [6]:

$$\ln\left(P_{eq}\right) = A - \frac{B}{T} \tag{9}$$

Where, A and B are the constants. The values of constants are given in the table1.

2.6. Initial and Boundary Conditions

Initially the bed temperature, density and pressure in the storage device are assumed to be constant.

$$T = T_o, \rho = \rho_o, P = P_o \tag{10}$$

Values of T_o, ρ_o and P_o depend upon absorption/desorption process.
Adiabatic boundary conditions are applied at all exterior surfaces.

$$\left(-k\,\frac{\partial T}{\partial n}\right) = 0 \tag{11}$$

Convection boundary condition is valid at heat exchanger tube wall. Therefore,

$$\left(-k\frac{\partial T}{\partial n}\right) = h(T_f - T_{wall}) \tag{12}$$

In the Eq. (12), $\vec{n}$ represents the unit normal vector for the corresponding wall.
Storage capacity of the device is given as follows:

Storage capacity (wt%) = [(Mass of H_2 absorbed)/(Mass of MH used)]×100

Thermo-physical properties of materials used in numerical simulation are given in table 1.

Table 1: Thermo-physical properties of materials used in model.

Sl. No.	Parameters	$LaNi_5$	Hydrogen	Steel	Copper
1.	Porosity, ε (-)	0.5	-	-	-
2.	Initial density, ρ_{alloy} (kg m^{-3})	8200	.0838	7850	8700
3.	Specific heat, c_p (J kg^{-1} K^{-1})	419	14890	420	385
4.	Thermal conductivity, k (W m^{-1} K^{-1})	1.2	.18	19	400
5.	Reaction heat of formation, ΔH(J mol^{-1})	-30780	-	-	-
6.	Material constant, C_a (s^{-1})	59.187	-	-	-
7.	Activation energy-Absorption, E_a (J mol^{-1})	21179.6	-	-	-
8.	Universal gas constant, R (J kg^{-1} K^{-1})	-	8.314	-	-
9.	Material constant, C_d (s^{-1})	9.57	-	-	-
10.	Activation energy-Desorption, E_d (J mol^{-1})	16450	-	-	-
11.	Van't Hoff constants , A and B (K)	12.99, 3704.59	-	-	-
12.	Initial concentration of bed, c_0 (mol m^{-3})	18981.48	-	-	-

3. Simulation Methodology

3-D geometry of the storage devices are built and solved using COMSOL Multiphysics 4.3b for comparing the results. COMSOL Multiphysics is specialized in solving the combined heat and mass transfer problems in porous medium. Except design 6, quarter part of every design is solved to save the time. Different global parameters, variables and constants are allocated. There are three different physics involved inside the reactor. According to these physics, suitable modules of COMSOL Multiphysics are used in the numerical model. The governing equations of these modules represent the physics. Sorption process in the hydrogen storage device is the transient phenomenon and also depends upon spatial coordinates. Therefore, time dependent PDEs are used to represent the numerical model. COMSOL Multiphysics uses finite element method (FEM) to solve these equations. Suitable initial and boundary conditions are imposed. Appropriate material

properties have been selected. An unstructured mesh of tetrahedral shape is generated by defining suitable maximum and minimum element size as well as growth rate. Mesh has been created according to the temperature and concentration gradient. Time dependent solver is used due to the transient problem. Absolute and relative tolerances have been given 10^{-6} and 10^{-4} respectively. A grid independence test is carried out for the accuracy of results.

4. Model Validation

For the model validation, the storage device geometry used by Singh et al. [1] is selected and numerical work is carried out accordingly. Behaviour of temperature and concentration profiles has the same trend as described in [1].

5. Results and Discussion

5.1. Absorption Process

Absorption process of hydrogen inside the storage device consisting of different HX designs is investigated at the operating parameters of 15 bar, 298 K and 0.113 Kg/s. Figure 3 shows the average bed concentration and temperature variation with respect to time for all the designs. During absorption process, hydriding is faster in the close vicinity of HX tube and pin fin surfaces so these areas are saturated earlier than the others. As time proceeds, reaction fronts move from these fin and tube surfaces to unsaturated regions. After some time, these reaction fronts meet each other and very less regions are left unsaturated. The absorption process of the hydrogen in a MH system follows a particular trend of curve which can be explained by dividing it into three different stages. These stages are described below.

Stage 1. It can be seen that at the beginning of the process, absorption rate of hydrogen increases rapidly up to a maximum value due to the existence of high driving potential (difference between hydrogen supply pressure and equilibrium pressure of bed) for mass transfer which leads to large amount of heat generation. Since, the bed temperature depends upon the absorption rate of hydrogen, it also follows the same trend. Stage1 has very short period of time. For example, device consisting of design 2 takes only 16 s to absorb 0.28 wt% of hydrogen in this stage and the peak temperature is 346 K.

Stage 2. Due to very poor thermal conductivity of metal hydride, generated heat is stored in the bed itself and increases the bed temperature as well as equilibrium pressure which reduces the absorption rate. It gives rise to heat and mass transfer crisis inside the storage device therefore transition takes place from stage 1 to 2. In stage 2, since bed temperature increases, the temperature difference between bed and heat transfer fluid also increases. This temperature difference enhances the heat transfer rate inside the device and decreases the bed temperature slowly up to end of the absorption process. More than 50% of hydrogen is absorbed in this stage. This region corresponds to the plateau of PCT-diagram. Form figure 3(b), it can be seen that in this region, hydride system have abrupt change in slope which happens due to the change in average reaction rate. Reaction rate changes primarily due to the larger bed thickness (distance between MH powder and cooling surface) and self-limiting nature of the metal alloy. To get fast reaction rates, heat should be transferred quickly. Larger bed thickness results in low heat transfer rate and reduces the reaction rate. The second reason for reduced reaction rate is the limited capacity of hydrogen absorption in a metal alloy. From figure 3(a), it can be seen that concentration profile for designs 1 and 5 is flatter than other designs due to higher bed thickness and reaches the saturation state in the last. The slope is approximately constant for design 6 due to constant average reaction rate (having very small and approximately constant bed thickness everywhere) throughout the 2^{nd} stage of the absorption process.

Stage 3. This is the final stage of the absorption process. In this stage, reaction rate slows down and bed temperature as well as pressure reaches to predefined initial conditions. Storage device equipped with design 2 approaches the cooling fluid temperature much faster than others and completes the absorption process in only 727s with its maximum storage capacity.

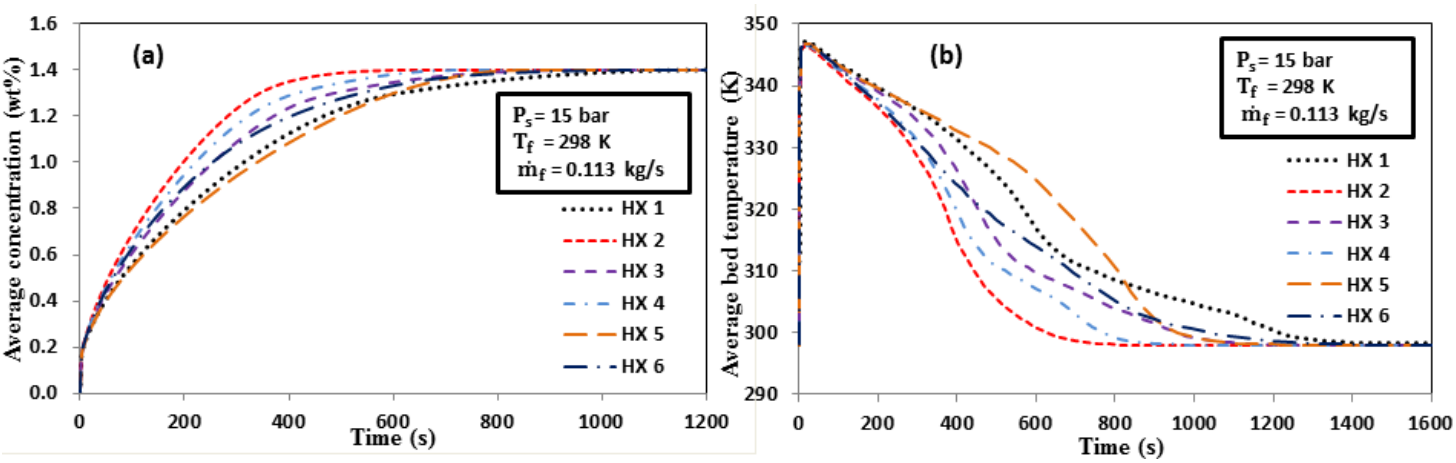

Fig. 3: Variation of (a) average bed concentration and (b) average bed temperature with time for all the HX designs.

5.2. Comparison of Performance for all the Heat Exchanger Designs

All the HX designs are solved numerically to reduce the cost of experiment. Performances of designs are compared on the basis of their geometry, charging time and volume occupied inside the container which is shown in table 2.

Table 2: Comparison of performances for all the HX designs.

Sl. No.	Parameter / Design	No. of tubes	Shape of pin fin	Type of pin fin attachment	Tube spacing (mm)	Pin fin length (mm)	Distributed mass flow rate (g/s)	Charging time for 1.2 wt% (s)	% Volume of vessel
1.	HX 1	16	Straight	Centre to centre	13	30	7.0625	470	4.0597
2.	HX 2	24	Straight	Centre to centre	10	18,36,38	4.7083	295	6.1076
3.	HX 3	24	Straight	Side by side	10	12,44,54	4.7083	370	5.7721
4.	HX 4	24	Straight	Side by side	10	12,44,54	4.7083	325	6.2709
5.	HX 5	17	Circular arc	Centre to centre	13.8592 (radial)	9.67 (arc length)	6.6470	505	4.2187
6.	HX 6	23	Spiral	Side by side	Random	4.25turns	4.9130	410	5.8018

It is found that storage device consisting of HX design 1takes 470 s to absorb 1.2 wt% of hydrogen. This design has four dead zones where bed thickness is higher. Due to this higher bed thickness, it is lacking in coupled heat and mass transfer process. To improve the performance of design 1, HX 2 is designed which takes only 295 s to absorb the same amount of hydrogen. Bed thickness is lower in design 2 which enhances the heat and mass transfer rate inside the storage device. Designs 1 and 2 are having centre to centre attachment of fins on the tubes. The second type of attachment is side by side attachment which is used in design 3 and 4. This type of attachment is mostly used in refrigeration industry due to ease of manufacturability. Design 3 uses side by side attachment of fins only in one direction while design 4 uses it in both the directions in the plane of fins. It is seen that time taken to absorb 1.2 wt% of the hydrogen is 370 s for design 3 whereas it is 325 s for design 4. All the designs discussed above are having straight pin fins. In our study, circular arc and spiral shape type pin fins are also used. Design 5 has circular arc type fins and these fins are centrally attached on tubes. It is observed that design 5 takes 35 seconds additional in comparison to design 1 to absorb 1.2 wt% of hydrogen. In the same manner, design 6 which has spiral shape pin fins takes 40 seconds more than design 3 to absorb 1.2 wt% of hydrogen.

Some other results are discussed below by selecting HX design 2 on the basis of the least charging time.

5.3. The Influence of Hydrogen Supply Pressure

Influence of supply pressure on average bed temperature and concentration has been observed at cooling fluid temperature of 298 K and velocity of 0.113 Kg/s which is shown in figure 4(a). In the figure 4(a), arrow tail to head portion

shows pressure increment. It has been found that larger supply pressure increases the pressure difference between supply pressure and equilibrium pressure which increases the overall reaction rate. Due to high reaction rate, bed saturates earlier in comparison to lower supply pressure and reduces the charging time of the device. It is seen that maximum value of the bed temperature also depends upon the supply pressure of the hydrogen. It occurs due to fast reaction kinetics and corresponding large amount of heat generation at higher supply pressure. The explanation regarding sharp rise in bed temperature and how it approaches to predefined initial fluid temperature slowly, is already given in the section (5.1). Evolution of bed concentration is shown in figure 4(b). It is seen that at time t = 420 s bed temperature and concentration are 312 K and 1.36 wt% respectively for 15 bar whereas these values are 315 K and .89 wt% for 5 bar supply pressure.

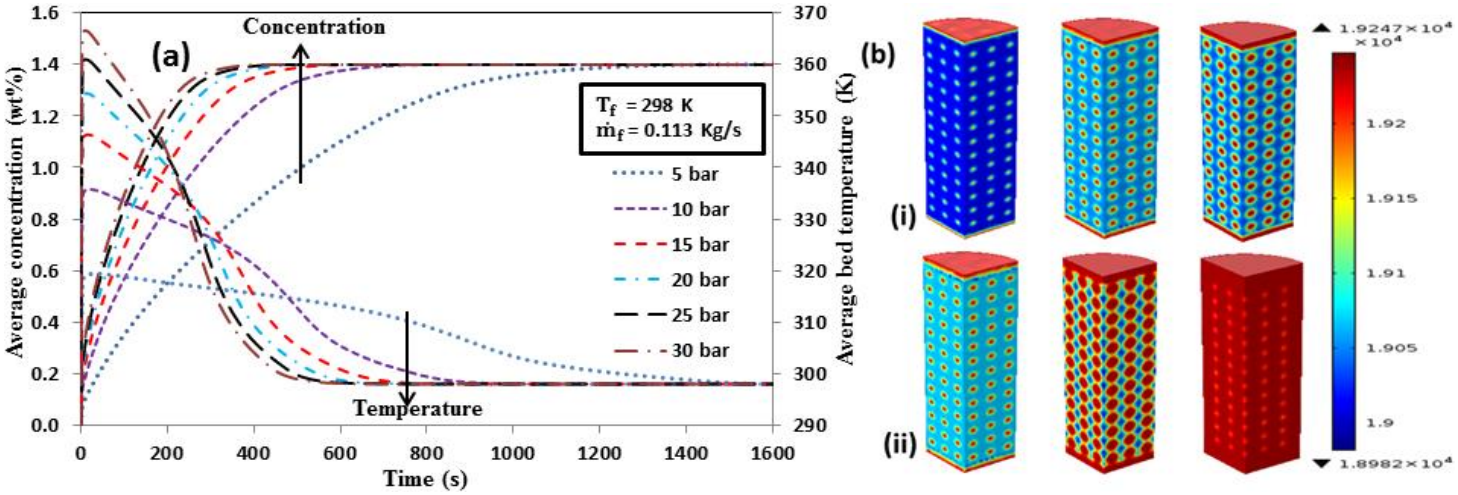

Fig. 4: Effect of H_2 supply pressure on (a) average bed concentration as well as temperature and (b) evolution of bed concentration at time t = 90, 270 and 390 s for (i) 5 bar (ii) 15 bar.

5.4. Bed Temperature and Concentration Profiles Along the Axial Distance

The axial variation of bed concentration as well as temperature during absorption process for different time intervals is shown in figure 5(a) and (b). Axial distance denotes distance from upper surface of top to bottom flange. Here, bed temperatures and concentrations are surface average value at a particular axial distance from top flange upper surface. From temperature and concentration plots, it can be seen that there are three regions, namely, upper, mid and lower region in the axial direction. Upper and lower regions of bed which are near the flange portions get saturated earlier than mid-region. It happens due to the fast removal of heat from nearby MH bed to the flange portion. In the mid region, there is no variation in bed temperature and concentration profile for a particular time interval.

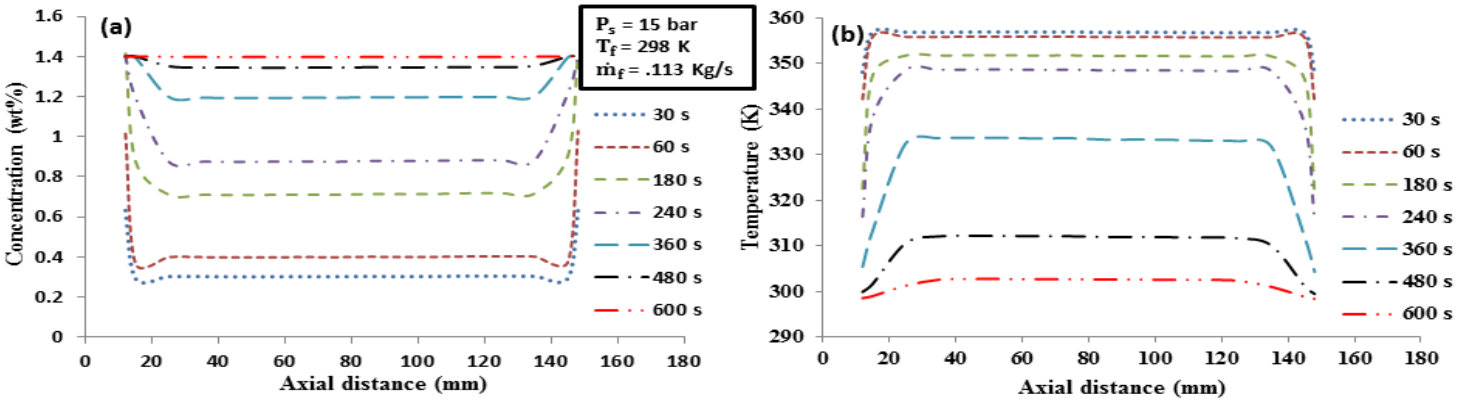

Fig. 5: Axial variation of bed (a) temperature and (b) concentration during absorption process at different time intervals

6. Conclusion

Simulation of the hydrogen storage device equipped with different designs of heat exchangers is carried out taking $LaNi_5$ as a MH alloy at the operating conditions of 15 bar, 298 K and 0.113 kg/s. All the designs are compared on the basis of their geometry, charging time and volume occupied inside the container. It may be concluded that geometry of design regarding number of tubes, shape, attachment and length of pin fin is important to select the good heat exchanger design for improving the charging time. Further in parametric analysis, it is found that higher supply pressure reduces the total absorption time of the device. It is also observed that mid part of the storage device is having constant temperature and concentration profiles at any time interval while lower as well as upper parts of the bed is saturated earlier than mid part.

Nomenclature

HX	heat exchanger	h	heat transfer coefficient, Wm^2K^{-1}	MH	metal hydride
P_s	H_2 supply pressure, Pa	T_f	fluid temperature, K	$\dot{m}_f$	fluid mass flow rate, Kg/s
C_p	specific heat, (J kg^{-1} K^{-1})	$\dot{m}$	mass rate of hydrogen, kg m^{-3} s^{-1}	t	time, s

Subscripts

a	absorption	d	desorption	eq	equilibrium
eff	effective	f	fluid	sat	saturation

References

[1] A. Singh, M. P. Maiya and S. S. Murthy, "Effects of heat exchanger design on the performance of a solid state hydrogen storage device," *International Journal of Hydrogen Energy*, vol. 40, no. 31, pp. 9733-9746, 2015.

[2] S. L. Garrison, B. J. Hardy, M. B. Gorbounov, D. A. Tamburello, C. Corgnale, B. A. vanHassel, D. A. Mosher and D. L. Anton, "Optimization of internal heat exchangers for hydrogen storage tanks utilizing metal hydrides," *International Journal of Hydrogen Energy*, vol. 37, no. 3, pp. 2850-2861, 2012.

[3] J. Ma, Y. Wang , S. Shi, F. Yang, Z. Bao and Z. Zhang, "Optimization of heat transfer device and analysis of heat & mass transfer on the finned multi-tubular metal hydride tank," *International Journal of Hydrogen Energy*, vol. 39, no. 25, pp. 13583-13595, 2014.

[4] H. Wang, A. K. Prasad and S. G. Advani, "Hydrogen storage system based on hydride materials incorporating a helical-coil heat exchanger," *International Journal of Hydrogen Energy*, vol. 37, no. 19, pp. 14292-14299, 2012.

[5] S. Mellouli, F. Askri, H. Dhaou, A. Jemni and S. Ben Nasrallah, "Numerical simulation of heat and mass transfer in metal hydride hydrogen storage tanks for fuel cell vehicles," *International Journal of Hydrogen Energy*, vol. 35, no. 4, pp. 1693-1705, 2010.

[6] G. Mohan, M. P. Maiya and S. S. Murthy, "Performance simulation of metal hydride hydrogen storage device with embedded filters and heat exchanger tubes," *International Journal of Hydrogen Energy*, vol. 32, no. 18, pp. 4978-4987, 2007.